

MIT Open Access Articles

Nanozyme-catalysed CRISPR assay for preamplification-free detection of non-coding RNAs

The MIT Faculty has made this article openly available. **Please share** how this access benefits you. Your story matters.

Citation: Broto, Marta, Kaminski, Michael M, Adrianus, Christopher, Kim, Nayoung, Greensmith, Robert et al. 2022. "Nanozyme-catalysed CRISPR assay for preamplification-free detection of non-coding RNAs." *Nature Nanotechnology*, 17 (10).

As Published: 10.1038/S41565-022-01179-0

Publisher: Springer Science and Business Media LLC

Persistent URL: <https://hdl.handle.net/1721.1/147986>

Version: Author's final manuscript: final author's manuscript post peer review, without publisher's formatting or copy editing

Terms of use: Creative Commons Attribution-Noncommercial-Share Alike



Nanozyme-catalysed CRISPR assay for preamplification-free detection of non-coding RNAs

Marta Broto^{1,†}, Michael M. Kaminski^{2,3,4,†}, Christopher Adrianus^{1,†}, Nayoung Kim¹, Robert Greensmith^{2,3}, Schan Dissanayake-Perera¹, Alexander J. Schubert^{2,3,4}, Xiao Tan^{5,6,7,8}, Hyemin Kim¹, Anand S. Dighe^{7,9}, James J. Collins^{5,8,10,*} and Molly M. Stevens^{1,*}

¹Department of Materials, Department of Bioengineering, and Institute of Biomedical Engineering, Imperial College London, London, U.K

²Berlin Institute for Medical Systems Biology, Max Delbrück Center for Molecular Medicine in the Helmholtz Association, Berlin, Germany.

³Department of Nephrology and Medical Intensive Care, Charité Universitätsmedizin Berlin, Berlin, Germany.

⁴Berlin Institute of Health, Berlin, Germany.

⁵Wyss Institute for Biologically Inspired Engineering, Harvard University, Boston, MA, USA.

⁶Division of Gastroenterology, Massachusetts General Hospital, Boston, MA, USA.

⁷Harvard Medical School, Boston, MA, USA.

⁸Institute for Medical Engineering and Science and Department of Biological Engineering, Massachusetts Institute of Technology, Cambridge, MA, USA.

⁹Department of Pathology, Massachusetts General Hospital, Boston, MA, USA.

¹⁰Infectious Disease and Microbiome Program, Broad Institute of MIT and Harvard, Cambridge, MA, USA

Email: jimic@mit.edu, m.stevens@imperial.ac.uk

[†]Authors contributed equally to the publication

*Corresponding authors

Abstract

CRISPR-based diagnostics enable specific sensing of DNA and RNA biomarkers associated with human diseases. This is achieved through the binding of guide RNAs to a complementary sequence which activates Cas enzymes to cleave reporter molecules. Currently, most CRISPR-based diagnostics rely on target preamplification to reach sufficient sensitivity for clinical applications. This limits quantification capability and adds complexity to the reaction chemistry. Here, we show the combination of a CRISPR/Cas-based reaction with a Nanozyme-Linked ImmunoSorbent Assay which allows for the quantitative and colorimetric readout of Cas13-mediated RNA detection through catalytic metallic nanoparticles at room temperature (CrisprZyme). We demonstrate CrisprZyme is easily adaptable to a lateral-flow-based readout and different Cas enzymes, and enables the sensing of non-coding RNAs including microRNAs, long non-coding RNAs and circular RNAs. We utilise this platform to identify patients with acute myocardial infarction and to monitor cellular differentiation *in vitro* and in tissue biopsies from prostate cancer patients. We anticipate that CrisprZyme has significant potential as a universally applicable signal catalyst for CRISPR-based diagnostics which will expand the spectrum of targets for preamplification-free, quantitative detection.

Introduction

Clustered regularly interspaced short palindromic repeats (CRISPR) systems and CRISPR-associated (Cas) enzymes function as an adaptive immune system in microbes and have been repurposed as diagnostic technologies in recent years¹⁻⁴. Here, sensing of DNA or RNA is mediated through a complementary guide RNA (gRNA), which induces the activation of a Cas enzyme that indicates the presence of a target analyte. To this end, a wide variety of assays have

been reported which differ in the usage of different Cas enzymes, reporter molecules or readout technologies. These assays have enabled the sensitive and specific detection of a wide range of pathogens,⁵ various biomarkers of human disease,^{6,7} and genetic variants,^{2,8} and have even been applied to the sensing of small molecules or proteins⁹.

However, most current CRISPR-based diagnostic methods rely on the preamplification of the target upstream of the CRISPR reaction. To this end, polymerase chain reaction (PCR)¹⁰ or isothermal amplification methods⁸ are commonly used. While these primer-based amplification techniques enable the detection of single DNA or RNA molecules in a reaction, PCR requires thermal cycling which limits its use as a point-of-care diagnostic, and isothermal amplification can suffer from complex primer design,^{8,11} non-specific amplification¹² and challenging quantification³. Moreover, the detection of specific mutations or sensing of very short target sequences, such as microRNAs (miRs), can restrict the design flexibility of an optimal gRNA, which requires methods for signal amplification. In addition, there is a critical need for versatile CRISPR-diagnostics that are easily adaptable to point-of-care readouts, work at ambient temperature and allow for usage with different Cas enzymes. Thereby, they could fully exploit the ease of use and programmability of this technology and enable quantitative sensing in resource limited settings.

Here, we report the development of CrisprZyme, the combination of a Cas-based reaction with a Nanozyme-Linked ImmunoSorbent Assay (NLISA) (Fig. 1). NLISA serves as a signal catalyst of reporter RNA detection; it is a stepwise addition of reagents onto an immobilised surface that ends with the catalysis of a substrate to generate a readout signal. The substrate conversion rate of nanozymes, which are comprised of nanometer-sized catalytic metallic particles, is higher than their enzymatic counterparts¹³, thus making NLISA even more sensitive than Enzyme-Linked ImmunoSorbent Assays (ELISA). Furthermore, NLISA offers high-throughput capability and ease of use. We designed nanozymes that are immobilised through an RNA linker oligonucleotide and can catalyse the oxidation of a chromogenic substrate. In the presence of the RNA target analyte, the RNA linker oligonucleotide gets degraded through Cas13-mediated collateral cleavage resulting in the absence of a colour change. We validated CrisprZyme using synthetic standards and RNA isolated from cell lines, patient tissue biopsies and plasma. We further adapted the assay for a lateral-flow-based readout and combined CrisprZyme with different Cas13 enzymes for enhanced sensitivity.

Main text

Nanozyme functionalisation and characterisation. We selected bimetallic nanozymes composed of platinum and gold (Pt@Au) due to their high catalytic activity¹³. Briefly, Pt@Au nanozymes were synthesised through a seed-mediated platinum overgrowth method using 15 nm gold nanoparticles as seeds, whereby polyvinylpyrrolidone (PVP) and L-ascorbic acid served as a stabiliser and a reducing agent for platinum, respectively¹³ (Fig. 2a). Next, we functionalised Pt@Au particles with a biotin-binding protein to bind them to the biotinylated reporter RNA. First, we tested different functionalisation procedures for optimal binding through the variation of pH,

protein concentrations and blocking agents. We found that pH 6.4-6.5, slightly above the isoelectric point of the biotin-binding protein (5 and 6.3 for streptavidin and neutravidin respectively), resulted in a higher signal-to-noise (S/N) ratio (Supplementary Fig. S1). This is because the slight positive charge of the protein interacts strongly with the negatively charged particles. Next, we aimed to improve the S/N ratio further by testing different biotin-binding proteins and blocking agents (Fig. 2b). From this, we selected a combination of streptavidin and phosphate-buffered saline solution containing 0.05% v/v Tween-20 (PBST) for higher S/N ratios. Protein blocking through addition of beta-casein or bovine serum albumin (BSA) was not required to avoid non-specific interaction between the particles and proteins on the NLISA plate. The particles were characterised by dynamic light scattering (DLS) to determine the functionalised particle size. The functionalised particles were found to be highly monodisperse, with a polydispersity index (PDI) below 0.074. Also, a ζ -potential change, from -44.3 mV to -25.6 mV, confirmed the presence of proteins on the surface of the particles.

To achieve the lowest limit of detection (LOD) of the reporter RNA concentration, calculated as EC_{10} , we tested the effect of nanozyme size. We first overgrew different amounts of Pt onto Au seeds to prepare particles with a range of diameters from 68 to 220 nm (Fig. 2c). Next, we performed a two-dimensional titration assay to select the best concentration of both anti-FAM and streptavidin-Pt@Au. The objective of the titration assay was to obtain a single monolayer of anti-FAM on the plate, found when the signal of the titration reaches assay saturation, and to obtain an absorbance of ~ 1 , selected arbitrarily outside the absorbance saturation range. We found 100 ng/mL of anti-FAM and 250 fM of streptavidin-Pt@Au to be the best combination (Supplementary Fig. S2). We then determined the optimal reporter RNA concentration, measured using these different particle sizes (Fig. 2d). We observed that a bigger particle size resulted in higher absorbance without compromising the LOD. Bigger particles enabled larger catalytic surface area per binding event, thereby increasing the detection capability. With this optimised assay design, using 188 nm particles, we achieved an LOD of 611 fM of reporter RNA. These optimised conditions were used in the experiments described below.

Transmission electron microscopy (TEM) and scanning transmission electron microscopy (STEM) brightfield (BF) images showed spherical nanoparticles of *ca.* 200 nm in diameter with nanometer-sized pores (*ca.* 1–2 nm) throughout the surface (Fig. 2e, Supplementary Fig. S3). The nanoscale pores are selectively accessible to small molecules (*e.g.*, H_2O_2) and significantly increase the surface area for catalytic amplification, as we previously reported¹³. On the other hand, functionalising with streptavidin did not induce any noticeable change to the overall morphology and size of Pt@Au. Notably, however, we observed that a thin layer of amorphous substance on the surface of Pt@Au was formed, which presumably indicates the successful functionalisation of the protein layer on the surface (Supplementary Fig. S4). We performed high-angle annular dark-field STEM (HAADF-STEM) that shows the atomic (Z) number contrast and applied energy dispersive X-ray spectroscopy (EDS) to analyse the elemental distribution in Pt@Au and streptavidin-Pt@Au (Fig. 2f–2g, Supplementary Fig. S5). The EDS elemental maps and intensity point/line profile analyses revealed that Pt and Au were present throughout the inner particle while Pt was the main element found in the periphery region.

Optimisation of the NLISA. Next, we incorporated the streptavidin-Pt@Au into the NLISA system. This assay consisted of four sequential steps: the addition of (1) antibodies directed against 6-carboxyfluorescein (anti-FAM), (2) the reporter RNA conjugated with a FAM and a biotin molecule at each end (5'-FAM-UUUUUC-Biotin-3'), (3) streptavidin functionalised nanoparticles (streptavidin-Pt@Au), and (4) a final addition of the chromogenic substrate, 3,3',5,5'-Tetramethylbenzidine (TMB), for colour development. The chromogenic substrate is a colourless solution that becomes coloured with absorption maxima at 450 nm once protonated with a sulfuric acid solution. Between each of the described steps, an extra wash step is performed with washing buffer (PBST), except after addition of the chromogenic substrate. The complex formed between the anti-FAM and streptavidin-Pt@Au through the reporter RNA determines its concentration. In this study, we used a four-parameter sigmoidal regression curve to process the data as described in Supplementary Equation S1.

RNA quantification using CrisprZyme. To develop a sensitive assay for the detection of target RNA, we next combined the NLISA quantification method with Cas13-based RNA detection (CrisprZyme, Fig. 1). For assay optimisation, we used a synthetic 71-nucleotide RNA as target analyte. In brief, a mastermix containing Cas13 from *Leptotrichia wadeii* (LwaCas13a), gRNA, and reporter RNA, was mixed with the target RNA to trigger the cleavage of the reporter RNA labelled with FAM and biotin. The reaction product was then added to the NLISA to quantify the amount of cleaved reporter RNA. Cleavage of reporter RNA occurred in the presence of target analyte, preventing the reporter RNA-mediated binding between the anti-FAM antibody and the streptavidin-functionalised nanozyme. The lack of binding reduces the linking of nanozyme particles, due to the removal of unbound particles during the wash step. This reduction in the number of particles resulted in a lower catalytic activity, and less chromogenic substrate oxidation. The presence of target analyte therefore inhibited colour development, whereas the absence of target increased the nanozyme-triggered colour change.

We first optimised the components of the reaction including buffers, enzyme and reporter concentrations (Supplementary Fig. S6). We observed that the reporter RNA concentration that showed the lowest LOD was 0.1 nM, which is more than two orders of magnitude lower than previously reported Cas13 assays¹⁴. We concluded that NLISA allowed for quantification of reporter RNA at lower concentrations than the fluorescent readout. Testing different ratios of gRNA to Cas13, we found a molar ratio of 1.2:1 (gRNA:Cas13) further increased sensitivity 10-fold. The optimised CrisprZyme assay allowed for the colour change that indicates different concentrations of target RNA to be observed by the naked eye (Fig. 3a). Quantification of the colour change with a plate reader showed a LOD of 4.72 pM through the measurement of absorbance at 450 nm (A_{450}) (Fig. 3b,g), while image analysis of the blue intensity in the central pixel of each well resulted in an LOD of 4.89 pM (Fig. 3c,g). Importantly, all LwaCas13a-based CrisprZyme assays were fully run at ambient temperature. Next, we adapted CrisprZyme for the readout with a lateral flow assay (LFA) (Fig. 3d). Target RNA is mixed with the gRNA-Cas13 complex and reporter RNA in the CRISPR reaction. Subsequently, streptavidin-functionalised nanozymes are mixed with the CRISPR reaction product containing the biotinylated reporter RNA to form a complex. A test strip composed of a nitrocellulose membrane and an absorbent pad was preprinted with anti-FAM and used to draw the mixture by capillary action. This allowed the capture of the non-cleaved reporter RNA-nanozyme complex on the test line. When exposed to

the substrate solution, the nanozymes on the test line catalysed the substrate oxidation generating an insoluble black line. By quantifying the pixel density on the test line on the image taken using a smartphone (Fig 3e), we achieved a LOD of 12.45 pM (Fig 3f, g). It is noteworthy that β -casein blocking on the particles is required to minimise the non-specific binding of the LFAs.

To confirm the assay's simplicity, we next tested whether CrisprZyme could be run in both 96- and 384-well plates (Supplementary Fig. S7a), allowing for high-throughput applications. The presence of non-targeting RNA strands in the background RNA isolated from HEK 293T cells (Supplementary Fig. S7b) resulted in a decrease in sensitivity of one order of magnitude. The assay time of the nanozyme part of CrisprZyme was dependent on the readout technology ranging between 30 min for lateral flow to 90 min for the plate reader format (Supplementary Table S1). Combined with the Cas reaction (3 h) the total assay time was 3.5 h for lateral flow or 4.5 h for the plate reader. Further work should address shorter Cas reaction times followed by nanozyme-based readouts. Also, a full comparison of molecular diagnostic technology price (Supplementary Fig. S8) shows that our technology compares in consumable price to SHERLOCK and DETECTR strategies^{2,15}, without the requirement of purchasing small equipment like a heatblock.

Expanding the dynamic range of Cas13-based diagnostics. To assess target RNA concentrations amenable for quantitative detection, we tested different Cas13-based assays for their dynamic range. The conventional fluorescence-based Cas13 assay achieved an LOD in the pM range which is consistent with previously reported results¹⁶ (Supplementary Fig. S9). CrisprZyme showed an LOD of 7.88 ± 3.21 pM, (Fig. 4a, Table S2), and is comparable to other amplification-free strategies that require an electrochemical-powered readout⁶. Importantly, the LOD was similar when using lateral flow as readout or performing the reaction at room temperature underlining its potential for point-of-care applications. Furthermore, a shallow regression slope of -1.69 ± 0.30 would allow for the use of this technology in a quantitative format. Since various different Cas enzymes exist whose diverse properties can be leveraged for diagnostics, we next tested if CrisprZyme could be combined with LbuCas13a instead of LwaCas13a (Supplementary Fig. S10, Table S2). While the CRISPR reaction components need to be adapted to meet the requirements of LbuCas13a as previously described¹⁷, the nanozyme-based readout did not require modifications underscoring its versatility. Importantly, LbuCas13a increased the LOD of the assay to the femtomolar range (264.2 ± 0.16 fM), which further extends the spectrum of potential target analytes.

To further evaluate CrisprZyme's versatility, we investigated the additive combination of CrisprZyme catalysis and a preamplification step as described in the SHERLOCK technology². We included reverse transcription recombinase polymerase amplification (rt-RPA), followed by T7-based RNA transcription, Cas13 detection and NLISA. This enhanced the sensitivity to an LOD of 8.30 ± 0.97 fM (Fig. 4a, Table S2). However, due to exponential target amplification through rt-RPA, the slope was steeper (-4.07 ± 2.40) limiting its use in quantitative RNA detection and non-communicable diseases. Furthermore, despite the sensitivity enhancement of the NLISA for preamplification-free RNA detection, we discovered that the LOD of the preamplification-based assay is determined by rt-RPA's capability to create copies of the target analyte and inclusion of the NLISA thus does not necessarily reach a lower LOD.

Given the low LOD of CrisprZyme, we next tested if the assay could be employed for the detection of different non-coding RNA species since they represent promising biomarkers^{18–20} but can be challenging to sense^{21,22}. Indeed, CrisprZyme enabled the quantitation of synthetic standards of microRNA-223 (miR-223), aurora kinase A (AURKA) circular RNA and long non-coding RNA LIPCAR (lnc-LIPCAR) in the picomolar range (Fig. 4b). To test its correlation with an established quantitative diagnostic assay, we compared detection of miR-223 by CrisprZyme with rt-qPCR (Fig. 4c). Testing of five different samples containing miR-223 at concentrations between 20 pM and 400 pM revealed a high degree of correlation between the two assays, covering cycle threshold (C_t) values between 19 and 25 for rt-qPCR reactions.

Detection of ncRNAs in cell culture and human disease. To demonstrate the potential use of our developed assay, we applied it to sense different human ncRNAs (Fig. 5a). Since cell-type specific expression of miRs can serve as an indicator for cell fate conversion, we aimed to monitor *in vitro* differentiation from induced pluripotent stem cells (iPSCs) to cardiomyocytes through sensing of miR-143-3p (Fig. 5b). CrisprZyme successfully detected upregulation of miR-143-3p in induced cardiomyocytes without preamplification, which was in agreement with previous studies²³. To display the potential of CrisprZyme for the diagnosis of severe myocardial injury, we tested the blood of 59 patients presenting to the emergency department with chest pain for expression of lnc-LIPCAR (Fig. 5c). We observed upregulation of lnc-LIPCAR in patients with levels of high-sensitivity Troponin T (hsTNT) above 6 pg/mL as compared to a control group with levels lower than 6 pg/mL, indicating CrisprZyme's ability to identify patients with extensive myocardial infarction. Finally, circ-RNAs can be differentially expressed in human diseases and thereby serve as diagnostic biomarkers²⁴. Thus, we aimed to differentiate two prostate cancer types: neuroendocrine prostate carcinoma (NEPC) and prostate adenocarcinoma (ACA) by measuring expression of circ-AURKA. This has been identified previously as a marker of NEPC²⁴ (Fig. 5d). Since circ-AURKA expression is very low in ACA, we aimed for a qualitative assay that detected circ-AURKA in NEPC using rt-RPA and T7 transcription for preamplification of the target region followed by its detection through CrisprZyme. To specifically sense the circular isoform, we positioned the gRNA at the back-splicing junction and used divergent rt-RPA primer for preamplification. CrisprZyme detected circ-AURKA in total RNA isolates from 9 of 10 NEPC biopsies, while only 1 of 10 ACA biopsies were circ-AURKA positive.

Conclusions

We designed a nanozyme-based CRISPR-diagnostic assay, CrisprZyme, to accurately measure RNA concentration in complex samples by exploiting the high catalytic activity of Pt@Au nanozymes, which serve as signal catalysts for the cleavage of RNA reporter molecules. We functionalised the nanozymes with a biotin-binding protein and developed an NLISA that can measure reporter RNA concentrations down to fM concentrations.

CrisprZyme enabled the quantification of RNA targets at room temperature with an LOD in the low pM range. Since CrisprZyme is independent of the gRNA design and the specific Cas enzyme, it can be widely employed to amplify CRISPR-based diagnostics which rely on the collateral cleavage of reporter oligonucleotides. The assay is also amenable to a colorimetric readout that allows for detection by the naked eye, qualitative analysis through simple imaging, and

quantitative analysis with a spectrometer. These results indicate the versatility of CrisprZyme in resource-limited settings, while its adaptability to 96- or 384-well plates enables testing at large scale. In addition, CrisprZyme followed by lateral-flow based readouts facilitate the rapid analysis of samples at the point of care, while the combination with LbuCas13a allows for the quantitative preamplification-free sensing in the femtomolar range.

We showed that CrisprZyme allows the sensing of different non-coding RNA species including miRs, lncRNAs and circRNAs. We detected miRs indicative of cell differentiation from iPSCs to cardiomyocytes in cultured cell extracts. This presents CrisprZyme as an alternative approach to monitor cell differentiation in research laboratories. We also challenged CrisprZyme with the analysis of lnc-LIPCAR in blood from patients presenting with chest pain at hospital emergency rooms and circ-AURKA in tumor biopsies from patients with prostate cancer. Our results showed a significant difference between the patient cohorts and a clear performance capability for non-communicable diseases, indicating the diagnostic potential of CrisprZyme in complex clinical specimens.

CrisprZyme offers the possibility for the preamplification-free, quantitative detection of ncRNA species, and its combination with preamplification techniques allows for the qualitative sensing of RNA in the low femtomolar range. Future improvements of the assay will likely include a shorter assay time as well as the fast extraction of RNA from crude clinical samples, followed by Cas-mediated cleavage and nanozyme detection on a microporous nitrocellulose membrane substrate.

Acknowledgements

We acknowledge use of the characterisation facilities at the Harvey Flower Electron Microscopy Suite (Department of Materials, Imperial College London). We thank the Prostate Cancer Biorepository Network (PCBN) for providing patient samples. This work was supported by the Department of Defense Prostate Cancer Research Program, DOD Award No W81XWH-18-2-0013, W81XWH-18-2-0015, W81XWH-18-2-0016, W81XWH-18-2-0017, W81XWH-18-2-0018 and W81XWH-18-2-0019 PCRP Prostate Cancer Biorepository Network (PCBN). M.B. and M.M.S. acknowledge funding from the British Heart Foundation (RE/18/4/34215) and the EPSRC IRC in Early Warning Sensing Systems for Infectious Diseases (i-sense) Mobility Fund (EP/K031953/1). M.M.K. was supported by the German Academy of Sciences, Leopoldina (LPDS 2018-01) and the Emmy Noether Programme (KA5060/1-1). M.M.K. is a participant in the BIH Charité Clinician Scientist Program funded by the Charité – Universitätsmedizin Berlin, and the Berlin Institute of Health at Charité (BIH). C.A. was supported by the Singapore A*STAR National Science Scholarship (NSS) fellowship. A.J.S. was supported by the MD Research Stipend of the Berlin Institute of Health at Charité (BIH). H.K. and M.M.S. acknowledge funding from the Research Council of Norway through its Centres of Excellence scheme (262613). X.T. is supported by an American Gastroenterological Association Takeda Pharmaceuticals Research Scholar Award in Inflammatory Bowel Disease and the Wyss Institute. J.J.C. was supported by the Paul G. Allen Frontiers Group and the Wyss Institute. M.M.S. acknowledges funding from the EPSRC IRC in Agile Early Warning Sensing Systems for Infectious Diseases and Antimicrobial

Resistance (i-sense2) (EP/R00529X/1), the Royal Academy of Engineering Chair in Emerging Technologies award (CiET2021\94) and the Rosetrees Trust. We thank Anja Schütz and the team of the Protein Production & Characterization Technology Platform of the Max Delbrück Center for Molecular Medicine in the Helmholtz Association (MDC), Berlin, Germany (<https://www.mdc-berlin.de/protein-production-characterization>) for producing the LbuCas13a protein.

Author Contributions

M.B, M.M.K, J.J.C and M.M.S conceived and designed the research. M.B, M.M.K and C.A carried out all the experiments and analysed the data. N.K performed LFA experiments, TEM, STEM and EDX imaging and analyses. R.G and A.J.S performed rt-RPA, assisted in the design and production of gRNAs, and in the optimisation of LbuCas13a detection. S.D-P optimized and printed LFA strips. X.T collected patient samples and edited the manuscript. H.K performed cell differentiation. M.B, M.M.K, J.J.C and M.M.S wrote the manuscript with feedback from all the authors.

Competing Interests

M.M.S, M.B, C.A and S.D-P have filed a patent application (2110729.7) covering the techniques and assay design as described in the manuscript. J.J.C. is a co-founder and director of Sherlock Biosciences. The remaining authors declare no competing interests.

Figure Legends

Figure 1. CrisprZyme assay scheme. Schematic of the combination of a Cas-based reaction with a Nanozyme Linked ImmunoSorbent Assay (NLISA) proposed in this study. Target RNA is mixed with the gRNA-Cas13 complex and triggers collateral cleavage of reporter RNA. Subsequently, the mixture is added to an immunoassay plate precoated with anti-6-carboxyfluorescein antibody (anti-FAM). The unbound reporter RNA is washed away, and the nanozymes are added to form a complex through the bound reporter RNA. Finally, the substrate is added for colour development.

Figure 2. Pt@Au functionalised with streptavidin shows the best NLISA performance. **a**, Schematic showing the synthesis of Pt@Au. PVP: Polyvinyl pyrrolidone. **b**, Characterisation of the functionalised Pt@Au by S/N ratio and dynamic light scattering (DLS) with PBST and PBST supplemented with two different blocking agents: beta-casein and bovine serum albumin (BSA). Control corresponds to non-functionalised particles. Data points represent individual experiments. Error bars represent SD ($n > 3$ replicates). A_{450} : Absorbance measure at 450 nm. **c**, Number distribution of the hydrodynamic diameter of the Pt@Au prepared by overgrowing different amounts of Pt onto the surface of AuNP seeds or 120 nm Pt@Au. Data represent the mean \pm SD ($n = 3$ replicates). **d**, Sigmoidal regression curve of the reporter RNA with streptavidin-Pt@Au of different sizes. Data represent individual replicates ($n = 2$ replicates). A_{450} : Absorbance measure at 450 nm. **e**, Structural characterisation of non-functionalised and streptavidin-functionalised Pt@Au using transmission electron microscopy (TEM). Scale bar, 200 nm; 50 nm;

20 nm; (from left to right). **f-g**, STEM-Energy Dispersive X-ray Spectroscopy (EDS) analysis of streptavidin-functionalised Pt@Au. **f**, Representative high-angle annular dark-field (HAADF)-STEM image and EDS elemental mapping (Pt and Au). A merged image of Pt and Au maps is shown. Scale bar, 50 nm. **g**, Representative EDS spectra recorded from the whole area of the individual particle.

Figure 3. CrisprZyme detects synthetic RNA down to pM concentration. **a**, Photograph of CrisprZyme results in a 384-well plate; six replicates were performed for each concentration. Low concentration of target RNA to the left; high concentration to the right. **b**, Sigmoidal regression of the CrisprZyme of a lncRNA target. Data were obtained measuring the absorbance of each well with a plate reader at 450 nm (A_{450}). **c**, Sigmoidal regression of the CrisprZyme of a lncRNA target. Data were obtained taking a photo of the results and recording the blue intensity of each well set as a region of interest. **b,c**, Data represent the mean \pm SD ($n = 6$ replicates). **d**, Schematic of the combination of a Cas-based reaction with a nanozyme-amplified lateral flow assay proposed in this study. Target RNA is mixed with the gRNA-Cas13 complex and reporter RNA to trigger the CRISPR reaction. Subsequently, streptavidin-functionalised nanozymes were mixed with CRISPR reaction product containing the biotinylated reporter RNA to form a complex. A test strip preprinted with anti-6-carboxyfluorescein antibody (anti-FAM) was used to draw up the mixture. The uncleaved reporter RNA-nanozymes complexes were captured at the test line. Finally, the substrate is added for colour development. **e**, Detection of a serial dilution of lnc-LIPCAR with nanozyme-amplified lateral flow assay. Photographs show the test bands of the lateral flow test strips after completion of the assay without (top) and with (bottom) the substrate added for enhanced signal. **f**, Sigmoidal regression of the lnc-LIPCAR target for the nanozyme-amplified lateral flow assay. Data represent the mean of test line pixel density normalised to the internal grid lines of the light box. **g**, Sigmoidal regression curve parameters. The data have been extracted from the four-parameter equation (Eq. S1) used to fit the standard curve.

Figure 4: CrisprZyme expands the dynamic range of Cas13-based diagnostics enabling the quantitative sensing of different non-coding RNA species. **a**, Standard curves for the detection of serial dilutions of a lncRNA with CrisprZyme (blue) or combination of rt-RPA and CrisprZyme (orange). Data represent the mean \pm SD ($n = 6$ replicates). **b**, Comparison of the performance of CrisprZyme with different ncRNA targets, lnc-LIPCAR: long non-coding RNA LIPCAR, miR-223: microRNA 223, ncRNA: synthetic RNA, circ-AURKA: circular AURKA RNA. Data represent the mean \pm SD ($n \geq 3$ replicates). **c**, Detection of miR-223 with CrisprZyme (orange) or rt-qPCR (grey) in 5 different samples at the indicated concentrations. C_t : Cycle threshold for PCR reactions. Data represent individual replicates ($n \geq 2$ replicates). **a,b,c**, A_{450} Absorbance measured at 450 nm.

Figure 5: Quantification of different ncRNA species from cell culture and human plasma or tissue. **a**, Schematic representation of the sample analysis experimental workflow. **b**, Schematic of upregulated (red) miRs (grey) upon differentiation of induced pluripotent stem cells (iPSCs) to cardiomyocytes (CMs) *in vitro* (left). Expression of miR-143-3p in iPSCs and CMs as measured by CrisprZyme. ($N = 4$ samples, $n = 2$ replicates) **c**, Schematic of upregulated (red) lncRNAs (grey) in plasma of patients with heart failure. Expression of lnc-LIPCAR in patients with heart failure and a control group as measured by CrisprZyme. hsTNT: high sensitivity Troponin T. ($N \geq$

25 samples, n = 2 replicates). **d**, Schematic of upregulated (red) circRNAs (grey) in tissue biopsies from patients with prostate cancer. Expression of circular AURKA RNA (circ-AURKA) in biopsies of prostate adenocarcinoma (ACA) and neuroendocrine prostate carcinoma (NEPC) as measured by CrisprZyme. (N = 10 samples, n = 2 replicates) **b,c,d**. A₄₅₀: Absorbance measure at 450 nm. Data points represent the median of two replicates. Box and whiskers plots represent median and quartiles. Mann Whitney test.

Data Availability

Research data are available online at DOI: 10.5281/zenodo.6553774.

References

1. Pardee, K. *et al.* Rapid, Low-Cost Detection of Zika Virus Using Programmable Biomolecular Components. *Cell* **165**, 1255–1266 (2016).
2. Gootenberg, J. S. *et al.* Nucleic acid detection with CRISPR-Cas13a/C2c2. *Science* **356**, 438–442 (2017).
3. Gootenberg, J. S. *et al.* Multiplexed and portable nucleic acid detection platform with Cas13, Cas12a, and Csm6. *Science* **0179**, 1–10 (2018).
4. Harrington, L. B. *et al.* CRISPR-Cas12a target binding unleashes indiscriminate single-stranded DNase activity. *Science* **360**, 436–439 (2018).
5. Lee, R. A. *et al.* Ultrasensitive CRISPR-based diagnostic for field-applicable detection of Plasmodium species in symptomatic and asymptomatic malaria. *Proc. Natl. Acad. Sci. U. S. A.* **117**, 25722–25731 (2020).
6. Bruch, R. *et al.* CRISPR/Cas13a-Powered Electrochemical Microfluidic Biosensor for Nucleic Acid Amplification-Free miRNA Diagnostics. *Adv. Mater.* **31**, 1905311 (2019).
7. Kaminski, M. M. *et al.* A CRISPR-based assay for the detection of opportunistic infections post-transplantation and for the monitoring of transplant rejection. *Nature Biomedical Engineering* (2020) doi:10.1038/s41551-020-0546-5.
8. Li, L. *et al.* HOLMESv2: A CRISPR-Cas12b-Assisted Platform for Nucleic Acid Detection and DNA Methylation Quantitation. *ACS Synth. Biol.* **8**, 2228–2237 (2019).
9. Dai, Y. *et al.* Exploring the Trans-Cleavage Activity of CRISPR-Cas12a (cpf1) for the Development of a Universal Electrochemical Biosensor. *Angew. Chem. Int. Ed Engl.* **58**, 17399–17405 (2019).
10. Li, S.-Y. *et al.* CRISPR-Cas12a-assisted nucleic acid detection. *Cell discovery* **4**, 20 (2018).
11. Wong, Y.-P., Othman, S., Lau, Y.-L., Radu, S. & Chee, H.-Y. Loop-mediated isothermal amplification (LAMP): a versatile technique for detection of micro-organisms. *J. Appl. Microbiol.* **124**, 626–643 (2018).
12. Wang, D.-G., Brewster, J. D., Paul, M. & Tomasula, P. M. Two methods for increased specificity and sensitivity in loop-mediated isothermal amplification. *Molecules* **20**, 6048–6059 (2015).
13. Loynachan, C. N. *et al.* Platinum Nanocatalyst Amplification: Redefining the Gold Standard for Lateral Flow Immunoassays with Ultrabroad Dynamic Range. *ACS Nano* **12**, 279–288 (2018).

14. Kellner, M. J., Koob, J. G., Gootenberg, J. S., Abudayyeh, O. O. & Zhang, F. SHERLOCK: nucleic acid detection with CRISPR nucleases. *Nat. Protoc.* **14**, 2986–3012 (2019).
15. Kaminski, M. M., Abudayyeh, O. O., Gootenberg, J. S., Zhang, F. & Collins, J. J. CRISPR-based diagnostics. *Nat Biomed Eng* **5**, 643–656 (2021).
16. Abudayyeh, O. O. *et al.* RNA targeting with CRISPR–Cas13. *Nature* **550**, 280–284 (2017).
17. Shan, Y., Zhou, X., Huang, R. & Xing, D. High-Fidelity and Rapid Quantification of miRNA Combining crRNA Programmability and CRISPR/Cas13a trans-Cleavage Activity. *Anal. Chem.* **91**, 5278–5285 (2019).
18. Shi, T., Gao, G. & Cao, Y. Long Noncoding RNAs as Novel Biomarkers Have a Promising Future in Cancer Diagnostics. *Dis. Markers* **2016**, 9085195 (2016).
19. Beermann, J., Piccoli, M.-T., Viereck, J. & Thum, T. Non-coding RNAs in Development and Disease: Background, Mechanisms, and Therapeutic Approaches. *Physiol. Rev.* **96**, 1297–1325 (2016).
20. Wang, C. & Jing, Q. Non-coding RNAs as biomarkers for acute myocardial infarction. *Acta Pharmacol. Sin.* **39**, 1110–1119 (2018).
21. Zhu, C.-S. *et al.* Avenues Toward microRNA Detection In Vitro: A Review of Technical Advances and Challenges. *Comput. Struct. Biotechnol. J.* **17**, 904–916 (2019).
22. Dave, V. P. *et al.* MicroRNA amplification and detection technologies: opportunities and challenges for point of care diagnostics. *Lab. Invest.* **99**, 452–469 (2019).
23. Garate, X. *et al.* Identification of the miRNAome of early mesoderm progenitor cells and cardiomyocytes derived from human pluripotent stem cells. *Sci. Rep.* **8**, 8072 (2018).
24. Chen, S. *et al.* Widespread and Functional RNA Circularization in Localized Prostate Cancer. *Cell* **176**, 831–843.e22 (2019).

Methods

Recombinant production of LbuCas13a from *Leptotrichia buccalis* C-1013-b. The expression vector pC0072 LbuCas13a His6-TwinStrep-SUMO-Bsal was a gift from Feng Zhang (Addgene plasmid # 115267; RRID:Addgene_115267¹). The protein was produced using *E. coli* T7 Express cells (NEB) co-transformed with the pRARE2 plasmid. TB media was supplemented with 100 µg/mL ampicillin and 34 µg/mL chloramphenicol. The cultures were grown at 37 °C until the OD₆₀₀ reached approximately 2.0. Gene expression was induced by the addition of 0.5 mM isopropyl β-D-1-thiogalactopyranoside at 17 °C. After induction, cultures were grown overnight at 17 °C. Cells were harvested by centrifugation and the pellets were stored at -80 °C. For purification, cells were resuspended in lysis buffer (50 mM Tris pH 8.0, 0.5 M KCl, 5% glycerol, 1 mM MgCl₂), supplemented with cComplete™ (EDTA-free protease inhibitor cocktail, Roche), 0.5 mM dithiothreitol (DTT), 1 mM phenylmethyl-sulfonyl fluoride, and 6.000 U/mL lysozyme (Serva), and lysed by sonication (SONOPULS HD 2200, Bandelin Electronic GmbH & Co. KG). The extract was cleared by centrifugation at 36.000xg and the His6-fusion protein was captured from the supernatant using affinity chromatography on a 5 mL Ni Sepharose® 6Fast Flow column (Cytavia), equilibrated with 50 mM Tris-HCl pH 8.0, 0.5 M KCl, 5% glycerol, 1 mM MgCl₂, and 0.5 mM DTT. Before elution with elution buffer (20 mM Tris-HCl pH 8.0, 0.5 M KCl, 5% glycerol, 0.5 mM DTT, 0.2 M imidazole pH 8.0), the bound protein was washed three times with various wash buffers (1: 20 mM Tris-HCl pH 8.0, 1 M KCl, 5% glycerol, 0.5 mM DTT, 5 mM imidazole pH 8.0;

2: 20 mM Tris-HCl pH 8.0, 0.5 M KCl, 5% glycerol, 0.5 mM DTT, 5 mM imidazole pH 8.0; 3: 20 mM Tris-HCl pH 8.0, 0.5 M KCl, 5% glycerol, 0.5 mM DTT, 15 mM imidazole pH 8.0) to remove contaminating nucleic acids and proteins. The eluted protein was supplemented with 5% glycerol and 0.5 mM DTT, and the fusion tag was cleaved off by adding 1:75 (w/w) yeast Ulp1p SUMO protease. The protein was further purified by ion exchange chromatography on an HiTrap Heparin HP column (Cytavia), equilibrated with 20 mM Hepes-NaOH pH 7.5, 0.25 M KCl, 5% glycerol, and 1 mM DTT. The purification additionally included a size-exclusion chromatography step on a 26/600 Superdex 200 prep grade column (Cytavia), equilibrated with 50 mM Tris-HCl pH 7.5, 1 M NaCl, and 1 mM DTT. The storage buffer of the protein was adjusted to 50 mM Tris-HCl pH 7.5, 600 mM NaCl, 5% Glycerol, and 2 mM DTT. The purified protein was flash-frozen in small aliquots with liquid nitrogen and stored at -80°C until further use.

Buffers. RNase-free ultrapure distilled water (UPDW, Invitrogen) was used in all experiments. All buffers were prepared in RNase-free conditions. Phosphate buffer saline (PBS) is 0.01 M phosphate buffer in a 0.8% w/v saline solution, pH 7.5. Coating buffer is a 0.05 M carbonate-bicarbonate buffer, pH 9.6. PBST is PBS with 0.05% v/v Tween-20. Citrate buffer is 50 mM sodium citrate, pH 5.0. The substrate solution contains 0.01% w/v 3,3',5,5'-tetramethylbenzidine (TMB) and 0.02 % v/v H₂O₂ in citrate buffer. 10X Cleavage buffer is 200 mM HEPES, 600 mM NaCl, 90 mM MgCl₂, pH 6.

Pt@Au synthesis. 188 nm Pt@Au was synthesised by further overgrowing Pt onto 120 nm Pt@Au. The 120 nm Pt@Au preparation was described elsewhere². Briefly, 835 µL of UPDW, 165 µL of Pt@Au (120 nm, 500 pM), 20 µL of polyvinylpyrrolidone (PVP, 20% w/v, 10 kDa, Sigma), 40 µL of L-ascorbic acid (100 mg/mL, Sigma), 40 µL of H₂PtCl₆ x 6H₂O (100 mM, Sigma) was added into a 1.5 mL glass vial in this order of addition. It was vortexed and immediately incubated at 65 °C for 1 h. Pt@Au was then cooled to room temperature, and excess reagents were removed through three sequential washing cycles at 7000 g for 5 min with UPDW. The product was resuspended in UPDW to have a final volume of 165 µL of Pt@Au (500 pM).

Pt@Au characterisation. All batches of Pt@Au were diluted to 6.25 pM in UPDW and characterised using Zetasizer nano series ZEN3600 to measure the charge and particle size based on zeta potential and Dynamic Light Scattering (DLS), respectively. Transmission electron microscopy (TEM) imaging, scanning transmission electron microscopy (STEM) imaging, and energy dispersive X-ray spectroscopy (EDS) analyses were performed on a JEOL JEM-2100F field emission electron microscope operating at 200 kV, equipped with Gatan Orius SC 1000 CCD camera (2k x 4k), Gatan annular bright field (BF), Gatan high-angle annular dark-field (HAADF), and EDS detectors (Oxford Instruments INCA EDS 80 mm X-Max detector system with STEM capability). Prior to the imaging and analyses, the samples were prepared by placing a 2 µL droplet of the nanoparticle dispersion on a 200-mesh carbon-coated copper grid (Electron Microscopy Science, USA). AZtecTEM Software (Oxford Instruments) was used for all EDS data acquisition and processing, and TruMap™ mode in AZtecTEM was used for the elemental mapping.

Pt@Au functionalisation. Pt@Au was functionalised with streptavidin or neutravidin by mixing 200 µL Pt@Au (500 pM), 20 µL phosphate buffer (50 mM, pH 6.4) and 20 µL of biotin-binding protein (1 mg/mL). The mixture was shaken at 700 rpm for 3 hours at room temperature. 100 µL of blocking protein (beta-casein or BSA at 1 mg/mL) or PBST was added into the mixture. It was

then shaken at 700 rpm for 1 hour at room temperature. The excess reagents were removed through three sequential washing cycles at 7000 g for 5 min with PBST. The product was resuspended in PBST to have a final volume of 200 μ L of streptavidin-Pt@Au or neutravidin-Pt@Au (500 pM).

Nanozyme-linked Immunosorbent Assay (NLISA). A microtiter plate (384 wells, Maxisorp™, Nunc) was coated with anti-FAM antibody (100 ng/mL in coating buffer, 40 μ L per well, Abcam) for 3 hours at room temperature (r.t.) and covered with an adhesive plate sealer. The plate was washed three times with PBST (100 μ L per well), and 28 μ L of PBST was added per well followed by the solution containing the reporter RNA (5'-FAM-UUUUUC-Biotin-3', from 10 nM to 10 fM and 0 in PBST, 14 μ L per well) or the LwaCas13a reaction mixture (14 μ L per well). After 30 min at r.t., the plate was washed as before, and a solution of streptavidin-Pt@Au (0.5 pM in PBST, 40 μ L per well) was added to the wells and incubated for 30 minutes at r.t. The plate was washed again, and the substrate solution was added (40 μ L per well). Colour development was stopped after 30 min at r.t. with 4 N H₂SO₄ (20 μ L per well). Signal readout was plotted based on absorbance at 450 nm (Spectramax M5, Molecular Devices) or central pixel blue-intensity of each well measured using image software (FIJI on Surface Pro 4) of a photo of the plate (Samsung Galaxy Note 10 plus, 16 MP rear camera).

Target RNA. Synthetic target RNA was supplied by Integrated DNA Technologies. The RNA used in this study is summarised in Table S3. rt-RPA primers are complementary to the RNA target sequence. They were designed such that the forward primer is at the 5' end of the target site that is bound by the gRNA's spacer, while the reverse primer is at the 3' end. The forward primers also contain a T7 promoter sequence, enabling DNA amplicons to be first transcribed to RNA prior to Cas13-based detection. The primers were ordered as DNA (Table S4, Biomers).

gRNA production. LwaCas13a and LbuCas13a gRNAs, respectively, contained 28 and 20 nucleotide-long spacers complementary to the target site. For miRNA targets, spacers were designed to include the entire miRNA length. Constructs were ordered as DNA (Table S5, Biomers/ Eurofins) with an appended T7 promoter sequence for *in vitro* RNA transcription. Synthesis of gRNAs was performed using the HiScribe T7 Quick High Yield RNA Synthesis kit (New England Biolabs) according to the manufacturer's instructions and purified using the Monarch® RNA Cleanup Kit (50 μ g, New England Biolabs). DNA oligonucleotides containing a T7 promoter sequence served as templates. gRNA purity was checked using Bioanalyzer (Agilent) Small RNA Analysis Kit following the supplier's protocol.

CRISPR reaction. A Master Mix was prepared with a concentration of 3X of Cleavage buffer, 1.5 U/ μ L Murine RNase Buffer (New England Biolabs), 375 nM of RNase Alert V2 (Thermo Fisher Scientific), 135 nM of LwaCas13a (Genscript) and 67.5 nM gRNA. 10 μ L of synthetic RNA standards (from 1 μ M to 10 pM and 0, prepared in 10 ng/ μ L of PolyA RNA carrier) or samples were mixed with 5 μ L of LwaCas13 reaction Master Mix in a 384-well black clear-bottom plate (Corning) and let to react for 3 h at 25 or 37 °C. Fluorescence was measured at 490/520 nm each 5 minutes for 3 h (Spectramax M5, Molecular Devices).

When combined with NLISA (CrisprZyme), the Master Mix was prepared with a concentration of 3X of Cleavage buffer, containing 1.5 U/ μ L Murine RNase Buffer (New England Biolabs), 0.75 nM of 5'-FAM-UUUUUC-Biotin-3' (Integrated DNA Technologies), 300 nM of LwaCas13a (GeneScript) and 360 nM gRNA. 10 μ L of synthetic RNA standards (from 2000 pM to 0.5 pM and 0 pM, prepared in 10 ng/ μ L of PolyA carrier) or samples were mixed with 5 μ L of LwaCas13

reaction Master Mix in a 384-well PCR plate (Thermo Fisher Scientific) and let to react for 3 h at r.t. 14 μL were then provided as input for the NLISA. Reactions with LbuCas13a were performed similarly, with final concentrations of 10 mM Tris-HCl buffer, 10 mM NaCl, 1.5 mM MgCl_2 , 1 U/ μL Murine RNase Buffer (New England Biolabs), 1.25 ng/ μL HEK293T RNA, 0.1 nM of 5'-FAM-UUUUUC-Biotin-3' (Integrated DNA Technologies), 100 nM of LbuCas13a and 65.5 nM gRNA.

Lateral flow assay (LFA). The lateral flow strips with antiFAM test line were produced using an automated liquid dispenser (BioDot System AD3220). 0.5 mg/mL of filtered (0.2 μM filter) antiFAM antibody (Abcam 19224, lot GR175456-62) was dispensed at a height of 5 mm from the bottom of the nitrocellulose (CN95 Unisart® Nitrocellulose Membrane, Sartorius) before being dried overnight at 37 °C. Lateral flow half-dipstick assays were then assembled onto backing card (Kenosha, KN-PS1060.19) with overlapping absorbent pad material (Ahlstrom-munksjo, KN-222-20.1), before being cut into 4 mm wide test strips.

The LFAs were run in half-dipstick format by dipping the test strips into a 96-well plate (Corning #3641, flat bottom, non-binding surface) containing 10 μL of Cas reaction product, 50 μL PBST, 10 μL of streptavidin-functionalised Pt@Au (1 pM, blocked with beta casein). After the solution had fully wicked up the strip (ca. 10 min), the strip was then dipped in another well containing 100 μL of PBST for 10 min to wash through any unbound nanoparticles or reporter RNA. Subsequently, the strip was submerged in another well for 10 min filled with 330 μL (enough solution to cover test line on strip in well) freshly prepared PtNC substrate solution containing 38% 1X Pierce™ CN/DAB (4-chloro-1-naphthol/3,3'-diaminobenzidine, tetrahydrochloride) Substrate Kit (Thermo Scientific), 12% (w/w) hydrogen peroxide (Sigma), 50% (v/v) stable peroxide buffer. Finally, the strip was moved into a well containing 330 μL purified water for up to 10 mins to stop the reaction and was then briefly dried under ambient condition for ease of handling. Strips were imaged with an iPhone XS mobile phone camera. Test line intensities were quantified using ImageJ by first converting the image to grayscale (32 bit) before drawing a rectangle the width of the lateral flow strips and length long enough to include an internal control of one of the background grid lines. Using the gel analyzer tool, the pixel density of each test line was integrated before being normalised relative to the pixel density of the internal control.

rt-RPA rt-RPA was performed using the TwistAmp Basic Kit (TwistDx) as per the manufacturer's instructions and with the following modifications. The total reaction volume was 20 μL . First, 3.08 μL of RNA target and 1.92 μL of a 10 μM 1:1 mix of forward and reverse primers were heated for 10 min at 65 °C. A master mix was then prepared for the resuspension of TwistAmp Basic reaction pellets, where each pellet is to be resuspended with 29.5 μL Rehydration buffer, 2.05 μL UPDW, 0.95 μL Dithiothreitol (Sigma-Aldrich) at 1 M, 2.5 μL GoScript reverse transcriptase (Promega) at 160 U/ μL , and 2.5 μL MgOAc at 280 mM. 15 μL of the resuspended TwistAmp Basic reactions was added to each 5 μL RNA target-primer mixture, resulting in forward and reverse primers at 480 nM, Dithiothreitol at 19 mM, and GoScript reverse transcriptase at 8 U/ μL . Each reaction was incubated at 42 °C for 60 min.

rt-qPCR. miScript II RT Kit (Qiagen) was used for reverse transcription and miScript SYBR Green PCR Kit (Qiagen, miScript Primer Assay MS00003871) for qPCR following the supplier's protocol. Reverse transcription was performed with 10 μL of input, synthetic RNA standards (from 1000 to 0.1 fM and NTC, prepared in 1 ng/ μL of PolyA carrier) or samples in 0.2-mL PCR tubes. qPCR was performed with 1 μL as input in a 384-well PCR-plate on a QuantStudio™ 6 cycler

(ThermoFisher). Samples were interpolated using standard regression and samples with a concentration of miR-223 > 1 pM were selected and analysed by CrisprZyme.

Cell culture and cell differentiation. The human episomal iPSC line (Thermo Fisher) was maintained in the complete Essential 8™ medium (Thermo Fisher) on 6-well plates coated with Matrigel® (Corning) diluted in DMEM/F12 (Thermo Fisher). The cells were regularly split at a 1:12 ratio every 4 days using 0.5 mM EDTA. The medium was supplemented with 10 µM Rock inhibitor Y-27632 (STEMCELL Technologies) for the first 24 h after passaging to avoid cell dissociation-induced apoptosis. Cardiac differentiation was optimised from the previously reported protocol³ as follows: the iPSC medium was changed to the differentiation medium, RPMI supplemented with 2% v/v B27-insulin supplement (Thermo Fisher), 4 days after the split, when cells reached ~85% confluence. From day 0 to day 2, the differentiation medium was supplemented with 6 µM CHIR99021 (tebu-bio) and replaced with the fresh differentiation medium on day 2. From day 3 to day 5, the differentiation medium supplemented with 2.5 µM Wnt-C59 (Strattech) was applied. On day 5, medium was replaced with the fresh differentiation medium. Medium was switched to RPMI supplemented with 2% v/v B27 supplement (Thermo Fisher) on day 7 and replaced with fresh medium every other day. Spontaneous contraction of the cells was observed from day 7. Medium was switched to the RPMI without glucose supplemented with 2% v/v B27 supplement (Thermo Fisher) and 5 mM sodium lactate (Merck) and changed every other day for the metabolic selection of cardiomyocytes from day 11 to day 17. ncRNA was extracted on day 17 following the protocol described below.

Patient cohort. Plasma samples for the evaluation of Inc-LIPCAR were obtained from discarded material from clinical samples initially obtained from adults (> 18 years) presenting to Massachusetts General Hospital with chest pain and tested for high-sensitivity Troponin T (hsTnT). The material was excess to clinical needs and selected based on hsTnT values and storage at 4 °C for < 12 hours after initial blood draw. Plasma was then frozen at -80 °C prior to research use. The study was granted exemption from informed consent due to the use of anonymized discarded clinical samples and was approved by the Mass General Brigham IRB, Protocol #: 2019P002499.

RNA specimens extracted from tissue biopsies for the measurement of circ-AURKA were obtained through the Prostate Cancer Biorepository Network (PCBN), a US Department of Defense (DOD)/ Congressionally Directed Medical Research Program (CDMRP) bioresource. All samples were de-identified (MIT exempt determination E-1564). Primary adenocarcinoma samples were provided by Johns Hopkins University and neuroendocrine castration-resistant prostate cancer samples were provided by the University of Washington through RNA extraction of metastatic cancer tissue.

ncRNA extraction from samples. ncRNA was extracted from a cell pellet or 200 µL of blood using the miRNeasy Micro Kit (Qiagen) following the supplier's protocol. 3.5 µL of the Spike-In Control (Ce-miR-39, 1.6×10^8 copies/µL) was added after the QIAzol Reagent. ncRNAs were eluted from the RNeasyMinElute spin column with two washes of 14 and 8 µL of UPDW (total RNA > 30 ng/µL, A260/280 > 1). ncRNAs were diluted to 2.5 ng/µL of total RNA to be used as input for rt-RPA (3.08 µL) and LwaCas13a reaction (10 µL).

Data and statistical Analysis. All data analysis was conducted in GraphPad 9.0.0 (Prism). All the sample sizes and statistical tests are specified in the figure legends. Calibration curves were fitted to a four-parameter equation according to Equation S1, where maximum signal and

minimum signal are plateaus in the units of the Abs, EC50 is the concentration producing 50% of the maximal signal, and HillSlope is the slope at the inflection point of the sigmoid curve. Limit of detection (LOD) was defined as the 10% signal of the maximum signal. Results were normalised defining 0% as the smallest mean in each data set and 100% as the largest mean in each dataset.

1. Gootenberg, J. S. *et al.* Multiplexed and portable nucleic acid detection platform with Cas13, Cas12a, and Csm6. *Science* **0179**, 1–10 (2018).
2. Loynachan, C. N. *et al.* Platinum Nanocatalyst Amplification: Redefining the Gold Standard for Lateral Flow Immunoassays with Ultrabroad Dynamic Range. *ACS Nano* **12**, 279–288 (2018).
3. Burrige, P. W. *et al.* Chemically defined generation of human cardiomyocytes. *Nat. Methods* **11**, 855–860 (2014).

Supplementary Materials

Nanozyme-catalysed CRISPR assay for preamplification-free detection of non-coding RNAs

Marta Broto^{1,†}, Michael M. Kaminski^{2,3,4,†}, Christopher Adrianus^{1,†}, Nayoung Kim¹, Robert Greensmith^{2,3}, Schan Dissanayake-Perera¹, Alexander J. Schubert^{2,3,4}, Xiao Tan^{5,6,7,8}, Hyemin Kim¹, Anand S. Dighe^{7,9}, James J. Collins^{5,8,10,*} and Molly M. Stevens^{1,*}

¹Department of Materials, Department of Bioengineering, and Institute of Biomedical Engineering, Imperial College London, London, U.K

²Berlin Institute for Medical Systems Biology, Max Delbrück Center for Molecular Medicine in the Helmholtz Association, Berlin, Germany.

³Department of Nephrology and Medical Intensive Care, Charité Universitätsmedizin Berlin, Berlin, Germany.

⁴Berlin Institute of Health, Berlin, Germany.

⁵Wyss Institute for Biologically Inspired Engineering, Harvard University, Boston, MA, USA.

⁶Division of Gastroenterology, Massachusetts General Hospital, Boston, MA, USA.

⁷Harvard Medical School, Boston, MA, USA.

⁸Institute for Medical Engineering and Science and Department of Biological Engineering, Massachusetts Institute of Technology, Cambridge, MA, USA.

⁹Department of Pathology, Massachusetts General Hospital, Boston, MA, USA.

¹⁰Infectious Disease and Microbiome Program, Broad Institute of MIT and Harvard, Cambridge, MA, USA

[†]Authors contributed equally to the publication

*Corresponding authors

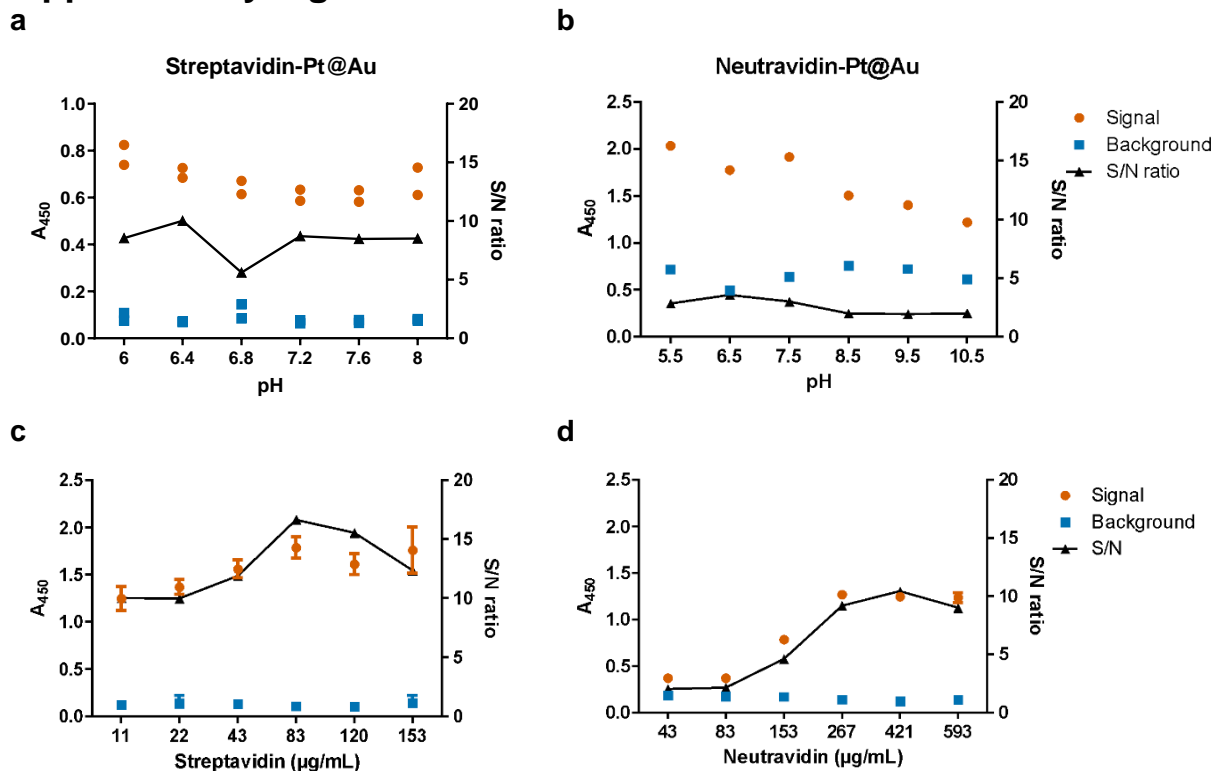
Supplementary Equation

$$Abs = Signal_{min} + \frac{Signal_{max} - Signal_{min}}{1 + 10^{(LogEC50 - Log(concentration)) \times HillSlope}} \quad \text{Equation S1}$$

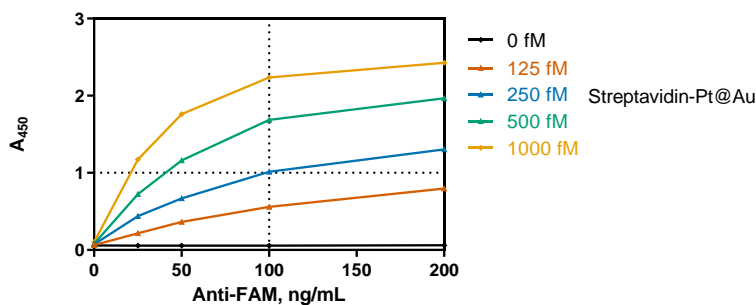
We used a four-parameter sigmoidal regression curve where the concentration of analyte is in log scale. The concentration of analyte is defined as the concentration of target RNA in a sample, to allow comparison of the concentrations reported here with other publications. This regression, Equation S1, defines the dynamic range of the assay between 10% (EC₁₀) and 90% (EC₉₀) of the

maximum and minimum signal. The hillslope describes the steepness and indicates the quantification capability, where a value close to 1 enables the best quantification accuracy.

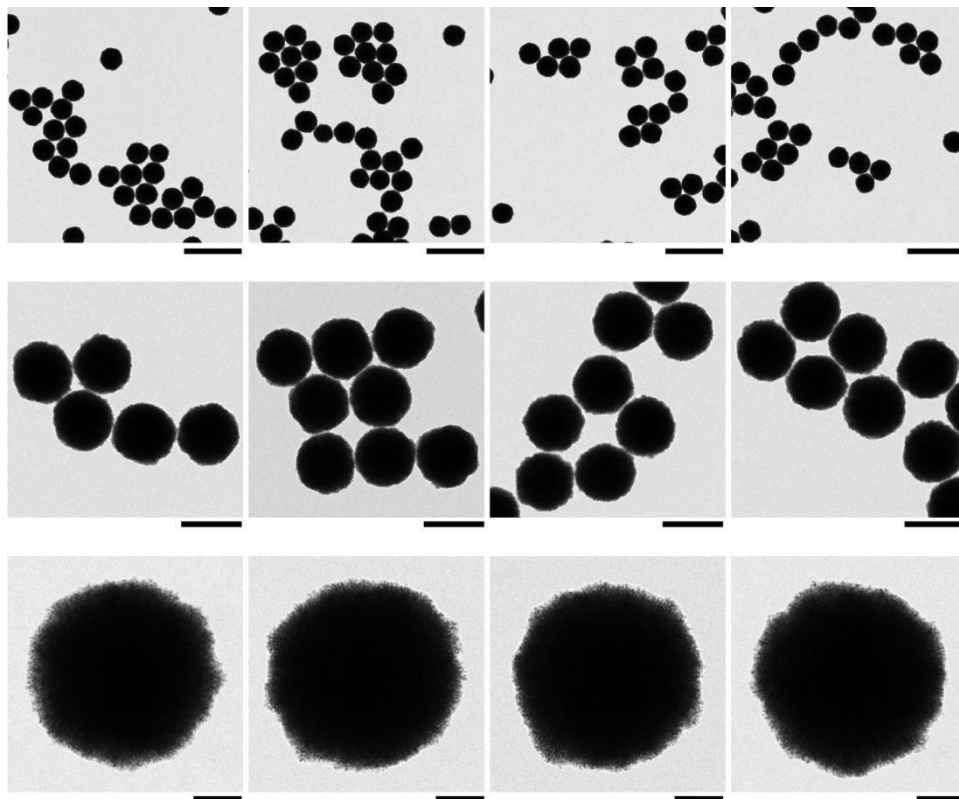
Supplementary Figures



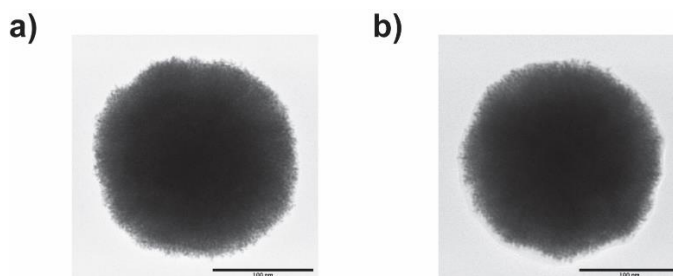
Supplementary Figure 1. Signal to noise (S/N) ratio achieved in the NLISA format with differently functionalized Pt@Au (streptavidin or neutravidin). **a,b**, Effect of different pH of buffers for the electrostatic interaction. Optimal pH, with highest S/N ratio, was observed at around pH 6.4-6.5. Data represents individual replicates. **a**, Streptavidin functionalized particles were added at 0.5 pM. **b**, Neutravidin functionalized particles were added at 1.25 pM. **c,d**, Different amounts of added protein for functionalization. Best performance, with highest S/N ratio, was observed with 83 $\mu\text{g/mL}$ of streptavidin and 421 $\mu\text{g/mL}$ of neutravidin. Data shown as mean \pm S.D. ($n = 3-4$). A_{450} : Absorbance measure at 450 nm.



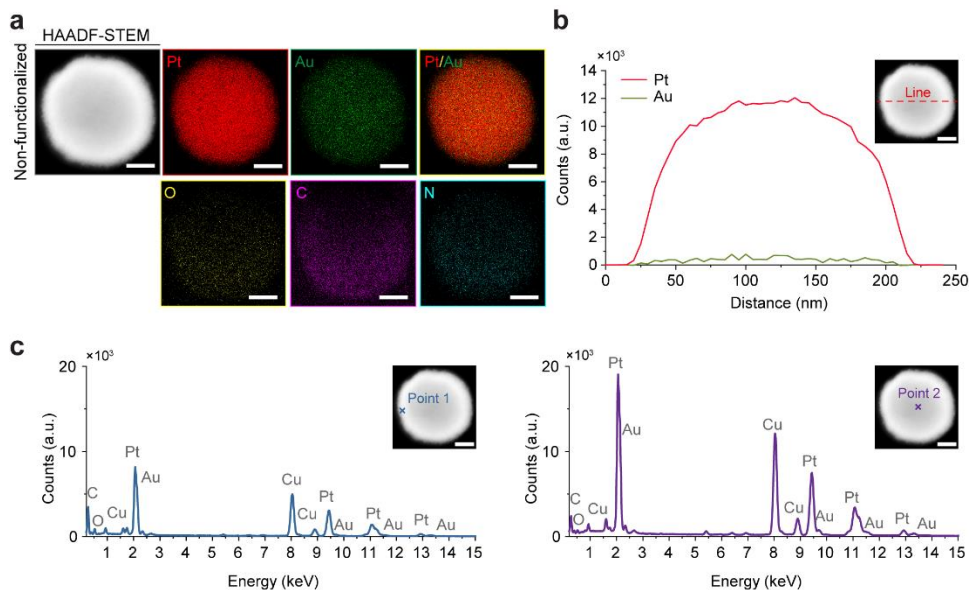
Supplementary Figure 2. 2D assay comparing anti-FAM and streptavidin-Pt@Au concentrations. Data represents single measurements. A_{450} : Absorbance measure at 450 nm.



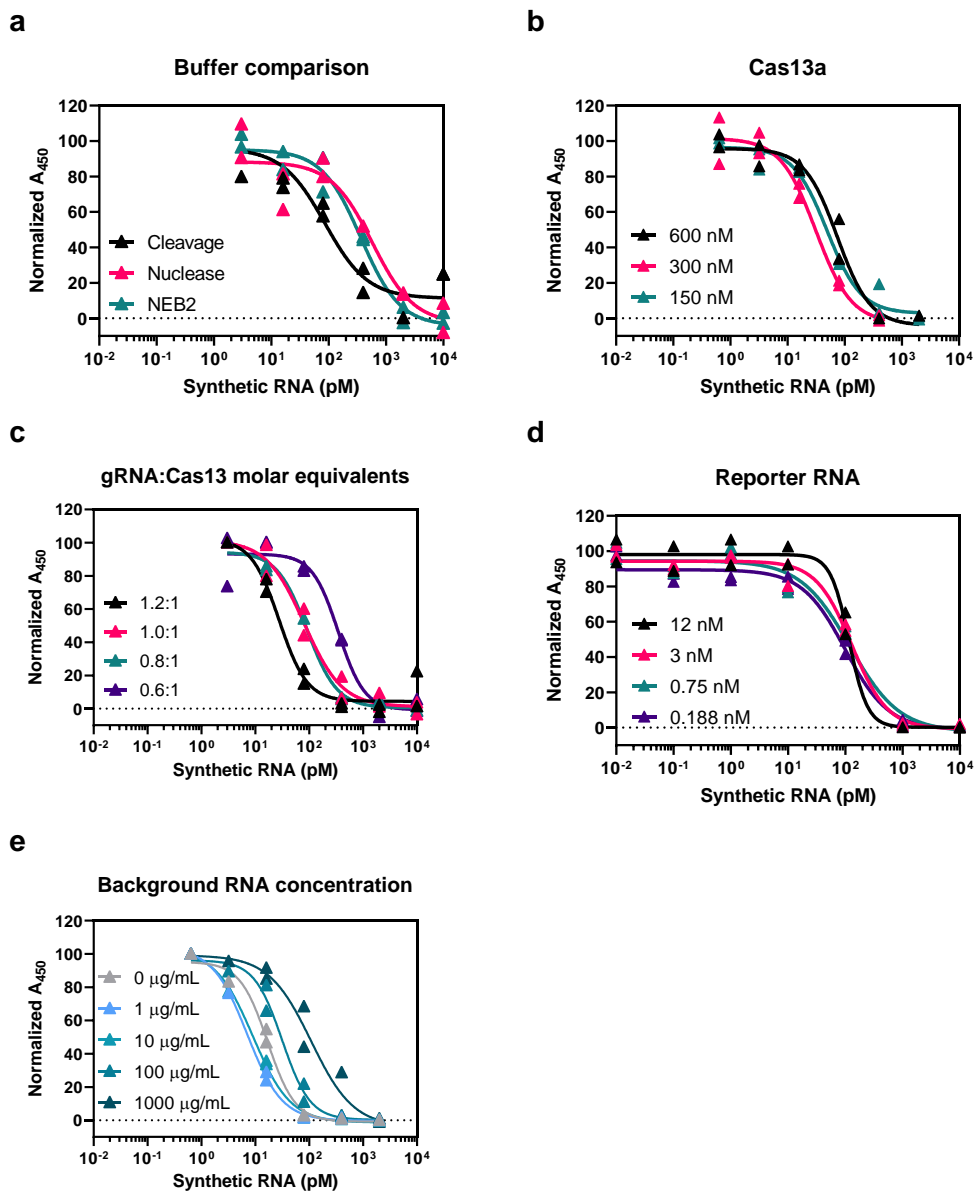
Supplementary Figure 3. Representative TEM images of streptavidin-functionalized Pt@Au. Scale bars, 500 nm (top); 200 nm (middle); 50 nm (bottom).



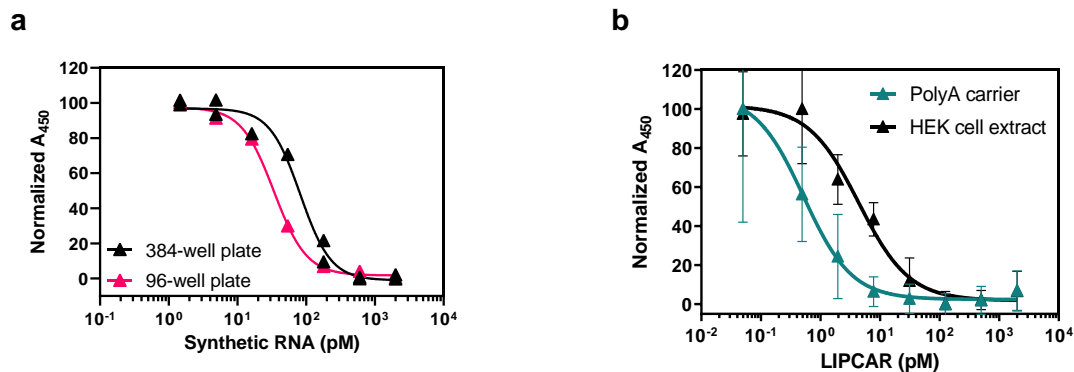
Supplementary Figure 4. Representative brightfield scanning-transmission electron microscopy (BF-STEM) images of (a) non-functionalised and (b) streptavidin-functionalised Pt@Au. Scale bar, 100 nm. There was no significant change in the morphology of the particles after the streptavidin functionalisation.



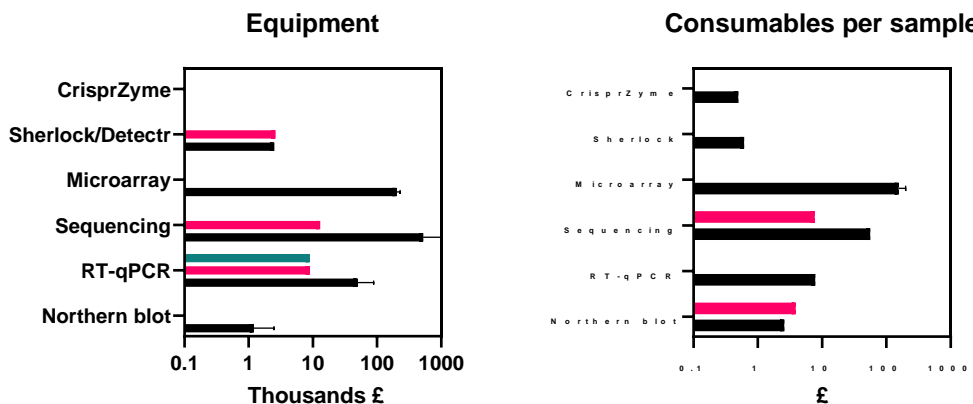
Supplementary Figure 5. Structural and elemental analysis of Pt@Au. **a**, Representative HAADF-STEM images and EDS elemental mapping (Pt, Au, O, C, N) of Pt@Au. Merged images of Pt and Au maps are shown. **b**, Intensity line profile across the HAADF image. **c**, EDS point spectra obtained from different regions on Pt@Au (periphery (point 1; left) and core (point 2; right)) that correspond to the x-marked positions on each image. Scale bar, 50 nm.



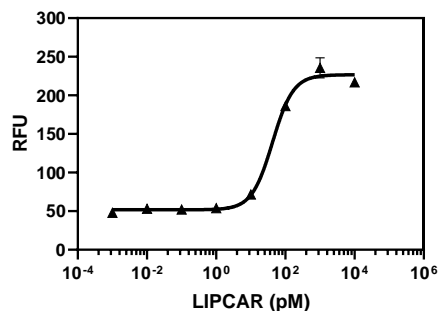
Supplementary Figure 6. Effect of different components on the performance of CrisprZyme. **a**, Effect of buffer salts in the mastermix. Cleavage buffer (20 mM HEPES, 60 mM NaCl, 9 mM MgCl_2 , pH 6), nuclease buffer (40 mM Tris-HCl, 60 mM NaCl, 6 mM MgCl_2 , pH 7.3), NEB2 buffer (10 mM Tris-HCl, 50 mM NaCl, 10 mM MgCl_2 , 1 mM DTT, pH 7.9) **b**, Effect of Cas13a concentration in the mastermix. **c**. Effect of the molar equivalents of gRNA:Cas13. **d**, Effect of the reporter RNA concentration in the mastermix. **e**. Effect of the presence of background RNA in spiked samples solution, polyA. **a,b,c,d,e**, Each experiment was conducted sequentially keeping the rest of parameters of the reaction constant. Data represents individual replicates ($n = 2$ replicates). Results were normalized defining 0% as the smallest mean in each data set and 100% as the largest mean in each data set. A_{450} : Absorbance measure at 450 nm.



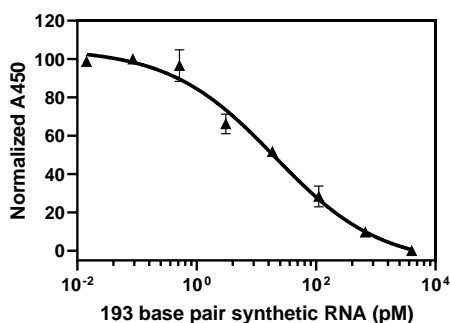
Supplementary Figure 7. CrisprZyme simplicity evaluation. **a**, CrisprZyme in different plate sizes. Data represents individual replicates ($n \geq 1$ replicates). **b**, CrisprZyme with other non-target RNA from HEK cells. Data and error bars represent mean \pm SD ($n = 6$ replicates). **a,b** Results were normalized defining 0% as the smallest mean in each data set and 100% as the largest mean in each dataset. A_{450} : Absorbance measure at 450 nm.



Supplementary Figure 8. Cost comparison of different molecular diagnostic technologies and CrisprZyme. Information and prices extracted from suppliers' websites. Sherlock and CrisprZyme price accounts for reagent price and not commercialised assay prices. CrisprZyme assay price is GBP190/364 reactions.



Supplementary Figure 9. LIPCAR detection based on fluorescence readout. Standard curve for the detection of serial dilutions of Inc-LIPCAR with LwaCas13a. RFU 490ex/520em: Relative fluorescent units after excitation at 490 nm wavelength and measurements of emitted light at 520 nm at room temperature. Data and error bars represent mean \pm SD (n = 3 replicates).



Supplementary Figure 10. CrisprZyme with LbuCas13a. LbuCas13a reaction was done at 37°C. Data and error bars represent mean \pm SD (n = 3 replicates).

Supplementary Tables

Table S1. Time comparison of time to run the proposed assays.

Assay timing	CrisprZyme	Lateral-CrisprZyme	rtRPA CrisprZyme
rtRPA			1 h
Cas13aRx	3 h	3 h	3 h
NLISA substrate	30 min	10 min	30 min
Particles	30 min	10 min	30 min
Development	30 min	10 min	30 min
Total assay time	4.5 h	3.5 h	5.5 h

Table S2. Sigmoidal regression curve parameters. Values represent mean \pm SD (n = 3 – 6 replicates). LOD: limit of detection.

Parameter, Mean \pm SD	Lwa-CrisprZyme	Lbu-CrisprZyme	rt-RPA-CrisprZyme
Hillslope	-1.69 \pm 0.30	-0.49 \pm 0.09	-4.07 \pm 2.40
Bottom	0.23 \pm 0.02	0.13 \pm 0.04	0.11 \pm 0.01
Top	1.19 \pm 0.04	1.06 \pm 0.02	1.12 \pm 0.01
EC ₉₀ (LOD)	7.88 \pm 3.21 pM	264.2 \pm 0.16 fM	8.30 \pm 0.97 fM
R ²	0.994 \pm 0.003	0.986 \pm 0.002	0.996 \pm 0.003

Table S3. Synthetic targets.

Target to be synthesised	Sequence (5' - 3')
Synthetic RNA	UGACGGGCGAGCUUUUGGCCCGGGUUAUACCUGA UGCUCACGUUAAGACGAGCAAAAAGCUUGUUGGUCA
miR-223	UGUCAGUUUGUCAAAUACCCC
Inc-LIPCAR	CAUGAUCACGCCUCAUAAUCAUUUUCUUAUCU GCUUCCUAGUCCUGUAUGCCCUUUUCCUAACACU CACAACAAAACUAAUACUAACAUCUCAGACG CUCAGGAAAUAGAA
circ-AURKA	GAAATTAATACGACTCACTATAGGTTTACAGGTAAT GGATTCTGACAAGGAAATTGCTGAGTCACGAGAAC ACGTTTTGGACCTCCAAGTGGAGCTGTAGCCAGTA GCAGTTCTCTGCTCATCAAACCTTTGAAAGTTTCTGA AGTTCTCTATAAACTGTTCCAAGTGGTGCATATTCC AGAATTAGG
193 base pair synthetic RNA	GAAATTAATACGACTCACTATAGGATCAAAGCACTTAC ATGAGGGGGCAAAGTCAGAGACAGCTGAGGAGCT GAAGAAGGTGGCTCAGGAGCTGGAGGAGAAGCTA AACATTCTCAACAATAAGATTCTGCAGGCGGACCAA GAACTGTGACCACAGGGCAGGGCAGCCACCAGGAG AGATATGCCTGGCAGGGGCCAGGACAAAATGCAAACCTT

Table S4. Primers.

Target	Primer	Sequence (5' - 3')
circAURKA	Forward	GAAATTAATACGACTCACTATAGGTTTACAG GTAATGGATTCTGACAAGGAAATTG
circAURKA	Reverse	CACTTGGAACAGTTTATAGAGAACTTCAGA
LIPCAR	Forward	GAAATTAATACGACTCACTATAGGTCATAATCATT TTCCTTATCTGCTTCCTAGTC
LIPCAR	Reverse	TATTTCCCTGAGCGTCTGAGATGTTAGTATTAG

Table S5. gRNA constructs.

Target	Sequence (5' - 3')
Synthetic RNA	GTTATACCTGATGCTCACGTATAAGACGGTTTTAGTCCC CTTCGTTTTTGGGGTAGTCTAAATCCCTATAGTGAGTCG TATTAATTTT
miR-223	TGTCAGTTTGTCAAATACCCCGTTTTAGTCCCCTTCGTTTT TGGGGTAGTCTAAATCCCTATAGTGAGTCGTATTAATTTT
Inc-LIPCAR	CTGTATGCCCTTTTCCTAACACTCACAAGTTTTAGTCCCCTTCG TTTTTGGGGTAGTCTAAATCCCTATAGTGAGTCGTATTAATTT
circ-AURKA	CAGTTCTCTGCTCATCAAACCTTTGAAAGGTTTTAGTCCCCTTCG TTTTTGGGGTAGTCTAAATCCCTATAGTGAGTCGTATTAATTTT
miR-143	TGAGATGAAGCACTGTAGCTCGTTTTAGTCCCCTTCGTTT TTGGGGTAGTCTAAATCCCTATAGTGAGTCGTATTAATTTT
193 base pair synthetic RNA	AGCTAAACATTCTCAACAATGTTTTAGTCCCCTTCATTTTT GGGGTGGTCCCTATAGTGAGTCGTATTAATTTT